

First and Second Order Topological Phases on Ferromagnetic Breathing Kagome Lattice

Arghya Sil^{1,*} and Asim Kumar Ghosh^{1,†}

¹*Department of Physics, Jadavpur University, 188 Raja Subodh Chandra Mallik Road, Kolkata 700032, India*

In this work, topological properties of a ferromagnetic Heisenberg model on a breathing kagome lattice are investigated extensively in the presence of Dzyaloshinskii-Moriya interaction. While the kagome ferromagnet hosts only a single first order topological phase, the breathing kagome system exhibits multiple first and second order topological phases along with their coexistence. Magnon dispersion relation is obtained by using linear spin wave theory. Flat band and Dirac cones are obtained in the absence of Dzyaloshinskii-Moriya interaction. A topological phase diagram is presented where several first and second order phases as well as their overlap are identified. Values of thermal Hall conductivity for all the first order phases are obtained. Distinct first order phases are characterized by different sets of Chern numbers in association with the necessary chiral edge states in accordance to the first order bulk-boundary-correspondence rule. Second order phase is characterized by polarization along with the emergence of corner states. Violation of the second order bulk-corner-correspondence rule has been noted in some regions.

PACS numbers:

I. INTRODUCTION

Topological states of matter have become one of the most studied topics for several years. A topological insulator (TI) is characterized by gapped bulk states and gapless boundary states or edge states. Time reversal symmetry (TRS) breaking TI's are known as Chern insulator¹, where each energy band is associated with a definite Chern number², while time reversal invariant TI's are characterized by a nontrivial Z_2 invariant³. Bulk-boundary-correspondence (BBC) rule^{4,5} determines the relation between the bulk and boundary properties of such systems and gives topological protection to the edge states. Also, there are topological crystalline insulators⁶, where mirror Chern number acts as the topological index.

Recently, the concept of higher order TI's (HOTI)⁷⁻¹² has been introduced where a d dimensional n -th order TI shows $(d-n)$ dimensional boundary states contrary to the conventional or first order TI's when $n = 1$. For instance, a two-dimensional second order TI (SOTI) will show zero-dimensional corner states but will not show one-dimensional gapless edge states¹³⁻²¹. In those HOTI's, the conventional BBC rule may not be applicable. Obviously, different types of topological invariants like polarization¹³, Z_Q Berry phase^{21,22}, nested Wilson loop⁸, mirror Chern number¹⁴ etc have been introduced depending on the symmetry of the system to characterize the topological property of the bulk. Origin of lower dimensional edge states can be attributed to quantization of dipole or quadrupole moment as observed in two-dimensional phononic and electric quadrupole topological insulators^{7,23,24}.

In recent times, besides electronic TI, topological magnon insulators (TMI)²⁵ are being studied, where the quasiparticle excitation (magnon) is bosonic in nature. It has been known that the topological nature of a system is independent of the statistics of the quasiparticles. Topological magnons are found before in honeycomb lattice^{26,27}, kagome lattice^{25,28}, Lieb lattice²⁹,

etc. Those topological phases have been experimentally observed in kagome ferromagnets, $\text{Lu}_2\text{V}_2\text{O}_7$ ^{30,31}, $\text{Cu}[1,3\text{-benzenedicarboxylate (bdc)}]$ ³², and honeycomb ferromagnet, CrI_3 ³³. Topological magnons give rise to thermal magnon Hall effect (MHE), in which a temperature gradient transports a dissipationless heat current which has been verified experimentally³⁴. Generally, in those spin systems, ferromagnetic (FM) Heisenberg model is considered where Dzyaloshinskii-Moriya interaction (DMI) is incorporated to trigger non-zero berry curvature. Spin models without DMI have also been shown to possess non-trivial topology. For example, FM Heisenberg models with Kitaev and spin-anisotropic interactions (HKSA) are found to host a number of topological phases^{35,36}. Thus, topological magnons have promising applications in the field of dissipationless spin transport, magnon spintronics and magnetic data storage.

On the other hand, HOTI's have been studied so far in fermionic systems in terms of tight-binding models on square and cubic lattice^{7-9,12}, breathing kagome^{13,37}, photonic systems^{19,38}, non-Hermitian systems¹⁶, etc. In addition, Kitaev model on Shastry-Sutherland lattice and magnetic vortex model on kagome lattice exhibit HOTI phases^{17,18}. Higher order topological Mott insulating phase has been demonstrated in a Hubbard model on the kagome lattice, where the topological state is characterized by Z_3 spin-Berry phase³⁹. Besides, SOTIs have been experimentally realized using quantized dipole or quadrupole polarization^{23,24} and implemented in mechanical systems²³, electrical circuits⁴⁰, microwave systems⁴¹, photonic⁴² and phononic crystals³⁷. However, no report on higher order topological phase in the FM Heisenberg systems is available till date.

In this work, we focus on the realization of second order topological magnon insulating (SOTMI) phase in a spin system with and without DMI. Here, FM Heisenberg model is formulated on the breathing kagome lattice in the presence of DMI along the nearest neighbor

(NN) bonds. The system reveals the existence of simultaneous first and second order TMI phases in different parameter regimes when DMI is non-zero. When DMI is zero, only second order TMI can be realized as the Chern number (C), the first order topological invariant, is always zero for all the bands. In other case, polarization is used as the bulk topological index to characterize the HOTI phase due to the mirror symmetry of the system¹³. So, polarization plays the crucial role to distinguish between the nontrivial and trivial SOTI phase in the same way C distinguishes between the nontrivial and trivial TMI phases in case of first order. One dimensional gapless edge states are found for nontrivial TI phase, while gapped edge states along with zero dimensional corner states are found for nontrivial SOTMI phase. For certain values of DMI strength, both type of phases are found to exist simultaneously. Transition between different topological phases are shown in the parameter-space. In addition, thermal Hall conductivity is calculated for all the TMI phases.

The article is organized in the following way. In section II, breathing kagome lattice is described and the linear spin-wave Hamiltonian is formulated. We describe the topological phases for zero DMI strength in the following section III. Topological phases for non-zero DMI strength are explained in the subsequent section IV. The values of thermal Hall conductivities are available in section V. Finally, section VI contains the discussion along with the summary of the results.

II. FORMULATION OF HEISENBERG HAMILTONIAN WITH DM INTERACTION

A FM Heisenberg Hamiltonian is formulated on the breathing kagome lattice with DMI along NN bonds. Breathing kagome lattice is composed of three identical triangular sublattices. As a result, the unit cell comprises of three sites A, B and C forming a downward triangle (Fig 1). The spin operators on those three sites are denoted by \mathbf{S}_n^a , \mathbf{S}_n^b and \mathbf{S}_n^c , respectively. The coordinates of a unit cell are denoted by $\mathbf{n} = (n_1, n_2)$. So, the Hamiltonian of this system can be written as

$$H = H_{\text{NN}} + H_{\text{mag}} + H_{\text{DM}}, \quad (1)$$

where

$$\begin{aligned} H_{\text{NN}} &= -J_\alpha \sum_{\langle n, n' \rangle} (\mathbf{S}_n^a \cdot \mathbf{S}_{n'}^b + \mathbf{S}_n^b \cdot \mathbf{S}_{n'}^c + \mathbf{S}_n^c \cdot \mathbf{S}_{n'}^a), \\ H_{\text{mag}} &= -h \sum_n (S_n^{az} + S_n^{bz} + S_n^{cz}), \\ H_{\text{DM}} &= -D_\alpha \sum_{\langle n, n' \rangle} (\mathbf{S}_n^a \times \mathbf{S}_{n'}^b + \mathbf{S}_n^b \times \mathbf{S}_{n'}^c + \mathbf{S}_n^c \times \mathbf{S}_{n'}^a) \cdot \hat{z}. \end{aligned}$$

J_α , $\alpha = 1(2)$ is the NN exchange interaction strength between upward (downward) triangles and D_α , $\alpha = 1(2)$ is the DMI strength, pointing towards z ($-z$) direction, between upward (downward) triangles. $\langle \cdot \rangle$ denotes the summations over NN pairs. Considering the FM case, we fix $J_\alpha > 0$ throughout the paper.

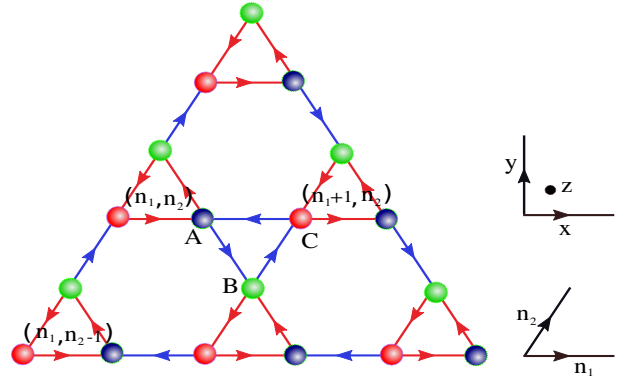


FIG. 1: (color online) A triangular replica of breathing kagome lattice is shown. Three sites A, B and C are denoted by green, blue and red spheres, respectively. The notation of the unit cells is also shown. The Heisenberg interaction strength is J_1 for the red lines (upward triangles) and J_2 for the blue lines (downward triangles). Considering DMI along z direction, coupling strength of two sites along the arrow will be $J_1 (J_2) + iD_1 (D_2)$ and opposite to the arrow will be $J_1 (J_2) - iD_1 (D_2)$. The lattice vectors, $\mathbf{n}_1 = (1, 0)$, $\mathbf{n}_2 = (1/2, \sqrt{3}/2)$ are shown in the side diagram.

$h = g\mu_B \mathcal{H}$, where \mathcal{H} is the strength of the external magnetic field along z direction, which helps to align the localized spins ferromagnetically along z direction when h is assumed greater than zero.

Now, based on the classical ground state in which all the spins point along the $+z$ direction, we obtain FM magnon dispersion relation by expressing the spin operators, \mathbf{S}_n^η , in terms of bosonic creation (η^\dagger) and annihilation operators (η) by using the standard Holstein-Primakoff (HP) transformation:

$$S_n^{\eta z} = S - \eta_n^\dagger \eta_n, \quad S_n^{\eta+} \simeq \sqrt{2S} \eta_n, \quad S_n^{\eta-} \simeq \sqrt{2S} \eta_n^\dagger,$$

where $\eta = a, b$ and c for the respective sublattices A, B and C. $S_n^{\eta\pm} = S_n^{\eta x} \pm iS_n^{\eta y}$. Now, following linear spin wave theory (LSWT) and using Fourier transformation of the operators in the form $\eta_n = \frac{1}{\sqrt{N}} \sum_{\mathbf{k}} \eta_{\mathbf{k}} e^{i\mathbf{k} \cdot \mathbf{n}}$ (N is the total number of unit cells in the lattice), the Hamiltonian in the momentum space can be written as

$$H = E_0 + H_{\text{SW}}, \quad (2)$$

where $E_0 = -h \sum_n S - 3(J_1 + J_2) \sum_{\langle n, n' \rangle} S^2$, is the classical ground state energy. H_{SW} can be written as (retaining terms only up to second order in bosonic operators)

$$H_{\text{SW}} = S \sum_{\mathbf{k}} \psi_{\mathbf{k}}^\dagger \mathcal{M}(\mathbf{k}) \psi_{\mathbf{k}}, \quad (3)$$

where $\mathbf{k} = (k_x, k_y)$, $\psi_{\mathbf{k}} = (c_{\mathbf{k}}, a_{\mathbf{k}}, b_{\mathbf{k}})$ and $\mathcal{M}(\mathbf{k})$ is a 3×3 matrix which is given by

$$\mathcal{M}(\mathbf{k}) = \begin{pmatrix} m_{11} & m_{12} & m_{13} \\ m_{12}^* & m_{22} & m_{23} \\ m_{13}^* & m_{23}^* & m_{33} \end{pmatrix}, \quad (4)$$

with the components, m_{ij} , given by

$$\begin{aligned} m_{11} &= m_{22} = m_{33} = 2(J_1 + J_2) + h/S, \\ m_{12} &= -(J_1 + iD_1) - (J_2 + iD_2)e^{-ik_1}, \\ m_{13} &= -(J_1 - iD_1) - (J_2 - iD_2)e^{-ik_2}, \\ m_{23} &= -(J_1 + iD_1) - (J_2 + iD_2)e^{i(k_1 - k_2)}, \end{aligned} \quad (5)$$

where $k_1 = \mathbf{k} \cdot \mathbf{n}_1 = k_x$ and $k_2 = \mathbf{k} \cdot \mathbf{n}_2 = k_x/2 + \sqrt{3}k_y/2$. Magnetic field only appears in each of the diagonal terms of $\mathcal{M}(\mathbf{k})$ with a fixed value, h/S , which means that topological properties of this system are totally insensitive to the value of \mathcal{H} . We have assumed a very small positive value of h only to ensure the FM ground state. As the Hamiltonian H_{SW} is number conserving, the magnon dispersion relation can be obtained by diagonalizing it. The results are valid for any value of S , while accuracy increases with the magnitude of S .

III. TOPOLOGICAL PROPERTIES WITH ZERO DMI

While kagome ferromagnet ($J_1 = J_2$) is topologically trivial in the absence of DMI, FM breathing kagome ($J_1 \neq J_2$) with zero DMI is found nontrivial. In this section, topological nature of the system will be discussed by studying both bulk and boundary properties of it in terms of suitable topological invariants to characterize them. Henceforth, the value of J_2 is fixed at unity while exploring the variation of topological phases with respect to the parameter J_1 . Three sets of bulk dispersion relation are shown in Fig 2 (a), (b) and (c), where $J_1 = 0.2$ for the region $0.0 < J_1 < 0.5$, $J_1 = 0.7$ for the region $0.5 < J_1 < 1.0$, and $J_1 = 1.0$, respectively. Note that the uppermost band is always flat and it touches the lower band at four corners of the Brillouin zone spanned by (k_1, k_2) , which are essentially the equivalent points. At this moment, the system is an insulator at $1/3$ filling as the lower two bands are separated. The gap decreases with the increase of J_1 and vanishes at $J_1 = 1.0$. The gap again opens up for $J_1 > 1.0$.

Below the bulk spectrum, we present the band structure of the corresponding finite strip of the system for every case. They are shown in Fig 2 (d), (e) and (f). The finite strip is prepared by breaking the periodic boundary condition (PBC) along the k_2 direction. In the region, $0.0 < J_1 < 0.5$, two gapped edge modes are found to exist between the lower two gapped bands, which do not decay into the bulk anymore. These are the signature of corner states, as proved in the previous studies^{13,14}. For $0.5 < J_1 < 1.0$, two edge modes are found to cross each other twice, without decaying into the bulk again. For $J_1 \geq 1.0$, there are no such edge modes. From this edge state spectrum, it is confirmed that the system is topologically trivial in first order since there is no gap between the upper two bands in the region $0.0 < J_1 < 1.0$. Instead, the system is found to host a nontrivial second order topological phase in the above region.

For the characterization of topological phases, bulk topological invariant has been formulated by following the procedure developed in the article¹³. In this formulation, a particular quantity, polarization along the n_i axis is defined by

$$p_i = \frac{1}{S} \iint_{1BZ} d^2\mathbf{k} A_i, \quad (6)$$

where $A_i = -i\langle\psi|\partial_{k_i}|\psi\rangle$ is the Berry connection with $i = 1, 2$ and $S = 4\pi^2$ being the area of the first Brillouin zone (1BZ) spanned by k_1 and k_2 . The set of polarization (p_1, p_2) is identical to the coordinates of the Wannier center¹³. The distance of the Wannier center from the origin can be taken as the bulk topological invariant as it changes its value only if the gap closes. For simplicity, we take p_1 as the topological index as it is protected by the mirror symmetry along the n_1 axis and it is also quantized. As we will see, it is non-zero in the topological phase and zero in trivial phase. It can be calculated analytically in extreme cases when either $J_1 = 0, J_2 \neq 0$, ($p_1 = 1/3$) or $J_2 = 0, J_1 \neq 0$, ($p_1 = 0$) as for the characterization of topological and trivial phases, respectively. For example, when $J_1 = 0, J_2 \neq 0$ the exact ground state wave function turns out to be $\psi = (1, e^{ik_1}, -e^{ik_2})^T/\sqrt{3}$. So, the Berry connection, A_1 , as well as polarization, p_1 , becomes equal to the value $1/3$, following the formula 6.

Values of p_i have been obtained numerically for every non-zero value of J_1, J_2 and DMI strength. To evaluate the integral, Eq 6, we discretize the Brillouin zone and redefine p_i as p_{in} (n being the band index) and A_i as $A_{in} = -i\langle\psi_{n\mathbf{k}}|\partial_{k_i}|\psi_{n\mathbf{k}}\rangle$. The value of p_{1n} has been calculated for every band, n . In this case, as the gapped edge states exist between the lower two bands, p_1 should have a quantized value for the lowest band. Numerical evaluation obtains the value of $p_1 = 1/3$ for $0.0 < J_1 < 1.0$, and $p_1 = 0$ for $J_1 > 1.0$, for the lowest band. Hence, the non-zero value of topological invariant confirms the nontrivial second order topological phase of the system for the region mentioned above.

In order to investigate the existence of corner states in this system, we consider a triangular replica of the breathing kagome lattice, as shown in Fig. 1, whose size is defined by the number of small triangles, L , along every edge. The triangular replica preserves the three-fold rotation symmetry, C_3 , of the breathing kagome lattice as well as it has the minimum number of corners, which is three in this case. Different shapes of the finite lattice can be considered for this purpose. In Fig 3 (a), we plot the energy spectrum as a function of J_1 for $L = 15$, which shows that corner states do exist for the region $0.0 < J_1 < 0.5$.

The numerical evaluation of the topological index p_1 shows that it bears the value $1/3$ for the entire region $0.0 < J_1 < 1.0$, which indeed should be the case as the insulating phase exists up to $J_1 = 1.0$ and the invariant has no scope to change its value since no phase transition occurs in the intermediate point. On the other hand, corner states cease to show its existence as soon as the gapped edge modes are found to cross each other.

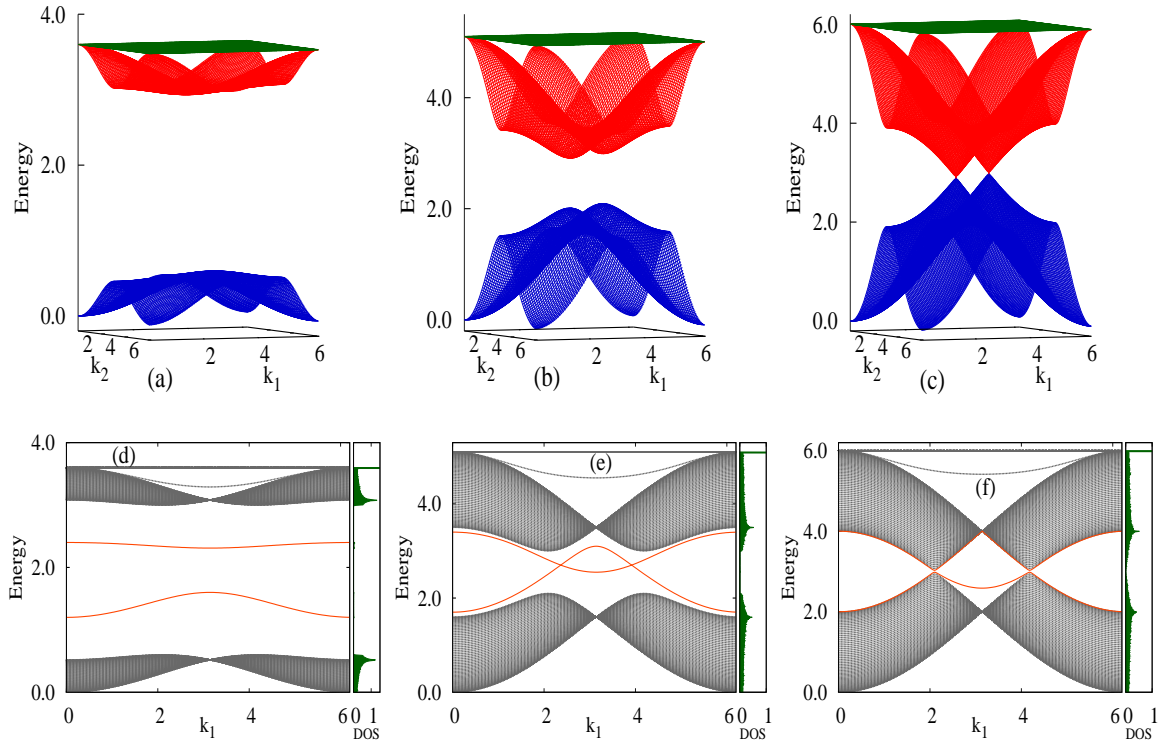


FIG. 2: (color online) Dispersion relation of breathing kagome system for zero DMI strength with $J_2 = 1$ and (a) $J_1 = 0.2$, (b) $J_1 = 0.7$, (c) $J_1 = 1.0$. Edge state diagram for finite lattice with 70 unit cells along k_2 direction with same parameter values as the corresponding bulk band structures in the upper row. The diagrams (d), (e) and (f) show the evolution of the in-gap edge modes (indicated by red lines) and depicts the way it affects the existence of corner states of the system. Density of states are shown in the side panel of each edge state diagram.

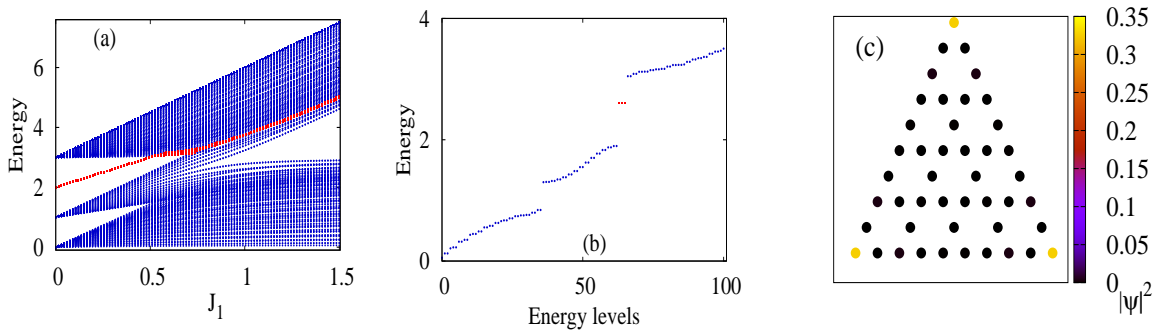


FIG. 3: (color online) (a) Energy spectrum of breathing kagome lattice with varying J_1 for $L = 15$. Upto $J_1 = 0.5$, zero dimensional corner states (indicated by red dots) show its existence and beyond this value, it seems to decay into the bulk. (b) Energy of the same system is plotted with respect to energy levels for $J_1 = 0.3$. Three red dots at same energy, $E = 2.6J_2$ show the states at the three corners of the finite triangle. The diagram is truncated to 100 energy levels (instead of 164 for $L = 10$) for better resolution of the three corner states. (c) Probability distribution of a particular eigenstate corresponding to a corner state energy for $J_1 = 0.2$ and $L = 5$. It shows that the states are indeed localized at the corners.

And it occurs in this system, when J_1 becomes greater than 0.5, which is illustrated in Fig 2 (e). As a result, no corner states are found beyond $J_1 = 0.5$. But, the system hosts the second order topological phase in the entire region $0.0 < J_1 < 1.0$, even though the corner states are topologically protected only up to $J_1 = 0.5$. It implies that bulk-corner-correspondence is satisfied for the region $0.0 < J_1 < 0.5$, and violated for the region $0.5 \leq J_1 < 1.0$. However, the system becomes trivial beyond the limit, $J_1 = 1.0$. In Fig 3 (b), the

energy spectrum is plotted with respect to the energy levels for a particular value of J_1 , which clearly shows the existence of three degenerate corner states at energy $2.6J_2$ which correspond to the three different corners of the triangular replica. The number of corner states may vary with the shape of replica with different number of corners. The distribution of probability density for a particular parameter value in this topological phase is shown in Fig 3 (c), which clearly exhibits that the corner states are truly localized at each corner.

IV. TOPOLOGICAL PROPERTIES WITH NON-ZERO DMI

The kagome ferromagnet ($J_1 = J_2$ and $D_1 = D_2$) exhibits a unique first order TMI phase in the presence of DMI²⁵. On the other hand, FM breathing kagome with non-zero DMI ($J_1 \neq J_2$ and $D_1 \neq D_2$) exhibits a rich topological phase diagram which includes distinct first and second order TMI phases as well as coexistence of both phases. In this section, effect of DMI on the topological properties will be discussed. DMI is turned on within upward and downward triangles with strengths D_1 and D_2 , respectively. For some specific values of J_1 , D_1 and D_2 , coexistence of both first and second order topological phases is found. Two such cases will be described extensively, where both edge and corner states are found simultaneously. Otherwise, distinct first or second order topological phases appear in different regions for the nontrivial cases.

Now, to characterize the first order topological phase, Chern number C_n for the n -th band has been evaluated which is defined as the integration of the Berry curvature, $\Omega_n(\mathbf{k})$, over the 1BZ, *i.e.*,

$$C_n = \frac{1}{2\pi} \iint_{\text{1BZ}} d^2\mathbf{k} \Omega_n(\mathbf{k}), \quad (7)$$

where $\Omega_n(\mathbf{k}) = -i(\langle \partial_1 \psi_{n,\mathbf{k}} | \partial_2 \psi_{n,\mathbf{k}} \rangle - \langle \partial_2 \psi_{n,\mathbf{k}} | \partial_1 \psi_{n,\mathbf{k}} \rangle)$. Here $|\psi_{n,\mathbf{k}}\rangle$ are the eigenvectors of $h(\mathbf{k})$ and $\partial_i = \frac{\partial}{\partial k_i}$. In this article, to calculate the Chern number, we use the discretized version of the integration, Eq 7, developed by Fukui and others⁴³. For nontrivial first order topological insulating phase, Chern numbers of two or more bands must be non-zero while it will be identically zero for all the bands for the trivial insulating phase. Chern numbers are undefined when the bands either touch or overlap. To confirm the existence of this first order topological phase, we construct the edge state energy diagram by breaking PBC along k_2 direction, diagonalizing the resulting Hamiltonian and plotting the energy spectrum with respect to the good quantum number k_1 . Likewise, for the characterization of second order topological phase, value of polarization is obtained in association with the prediction of corner states. To find the corner states a triangular replica of breathing kagome lattice with $L = 15$ is considered by breaking PBC along both the directions.

In the presence of DMI, the kagome ferromagnet exhibits a particular TMI phase with $C_n = (1, 0, -1)$ ²⁵. Numbering of band index follows the ascending order starting from the lowest energy. For FM breathing kagome, the uppermost flat band for zero DMI is found to become dispersive as soon as DMI is non-zero. The bulk dispersion relations plotted in Fig 4 (a), (b) and (c), with $D_1 = 0.1$ and $D_2 = 1.5$, reveal that the system is an insulator for this set of DMI in the region $0.00 \leq J_1 \leq 1.66$, as true gap exists between all the

bands. At a particular point, $J_1 = 1.67$, the upper band gap vanishes and reopens thereafter. Therefore the system undergoes a phase transition at $J_1 = 1.67$. Similar phase transition occurs at $J_1 = 1.92$ when the lower band gap vanishes.

Calculating C_n for each of the cases, it is found that $C_n = (-1, 1, 0)$ for $0.00 < J_1 \leq 1.66$. When $J_1 \geq 1.68$, the Chern numbers are redistributed as $C_n = (-1, 0, 1)$. Thus, the system undergoes topological phase transition through which the upper two bands exchange Chern number of ± 1 since the upper two bands touch at a Dirac band touching point. Similar situation happens again at $J_1 = 1.92$, where lower two bands touch at a Dirac band-touching point. At this time, they exchange Chern number of ± 1 leading to new distribution, $C_n = (0, -1, 1)$.

Fig 4 (d) shows chiral gapless edge states connecting the lower two gapped bands according to the BBC rule since the Chern numbers are $(-1, 1, 0)$. The pair of gapped edge modes in the upper band gap indicates the existence of corner states. But this time, they do not cross each other. Thus, there are simultaneous existence of first and second order topological insulating phases for $1/3$ and $2/3$ filling, respectively. In similar fashion, Fig 4 (e) and (f), correspond to the existence of other topological phases. The nature of edge states supports the pattern of Chern numbers for the corresponding parameter regions satisfying the BBC rule.

To confirm the presence of SOTMI phase, existence of the corner states is investigated. Fig 5 (a) shows the energy spectra with varying J_1 . It is evident that the SOTMI phase do exist up to $J_1 = 1.66$. The calculation of polarization further emphasizes our claim that TMI and SOTMI phase do simultaneously exist in the region $0.00 < J_1 \leq 1.66$. For this particular case, the topological invariant would be the value of p_1 of the uppermost band, since the gapped edge mode exist between the upper two bands. The value of p_1 remains fixed at $1/3$ for the whole region, which is same as the value of p_1 for zero DMI. But, in contrast to the zero DMI, here both corner states and non-zero polarization simultaneously persists for the region $0.00 < J_1 \leq 1.66$. This result can be implied from the fact that there is no crossover of in-gap edge modes in this insulating region. Thus, BBC as well as bulk-corner-correspondence rules are jointly satisfied both for TMI and SOTMI phases, as evident from the diagram. For $J_1 > 1.66$, the corner states decay into the bulk as well as polarization vanishes. Thus, SOTMI phase cease to exist beyond $J_1 > 1.66$.

This finding clearly predicts the existence of SOTMI phase as well as TMI phase in the region $0.00 < J_1 \leq 1.66$, when the strengths of DMI are fixed at $D_1 = 0.1$ and $D_2 = 1.5$. Therefore, DMI not only helps to extend the range of SOTMI phase from $0.0 < J_1 < 1.0$ to $0.00 < J_1 \leq 1.66$, in addition, it favors the coexistence of first and second order topological phases. The system undergoes a phase transition in the vicinity of $J_1 = 1.67$, hosting a new TMI phase thereafter.

A topological phase diagram is presented in Fig 6, which is drawn with respect to two parameters J_1 and

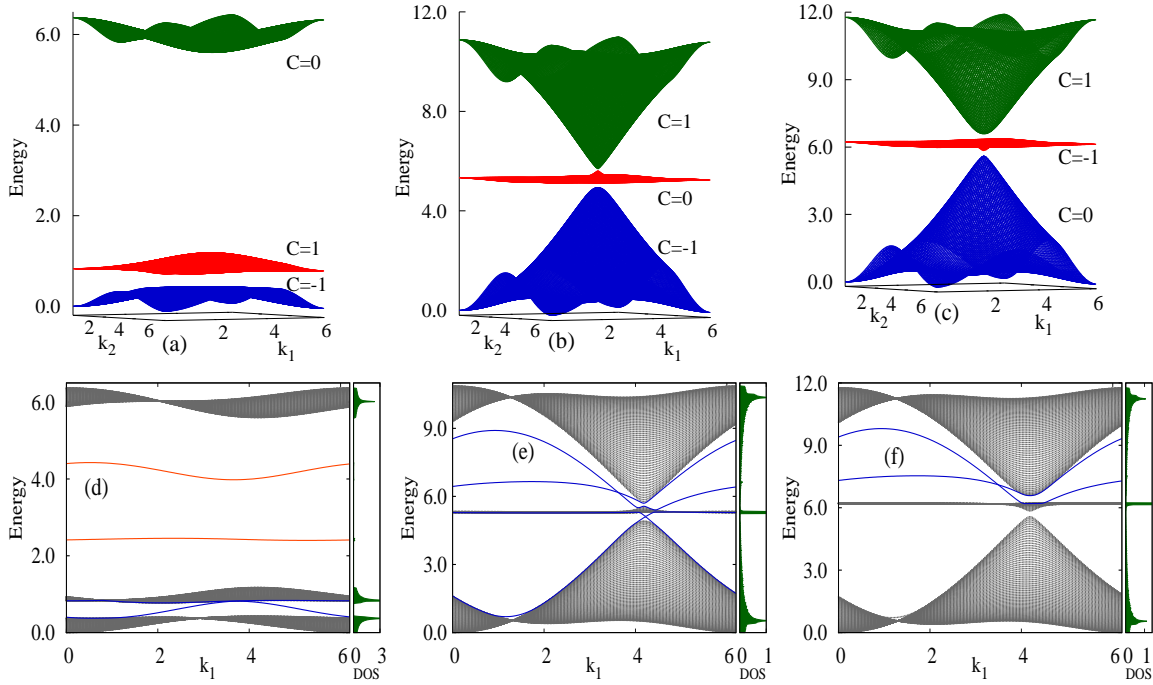


FIG. 4: (color online) Dispersion relation of breathing kagome system for non-zero DMI strength with $J_2 = 1.0$, $D_1 = 0.1$, $D_2 = 1.5$ and (a) $J_1 = 0.2$, (b) $J_1 = 1.7$, (c) $J_1 = 2.0$. Chern numbers of respective bands are also specified. Edge state diagram for finite lattice with 70 unit cells along k_2 direction with same parameter values as the corresponding bulk band structures in the upper row. The diagrams (d), (e) and (f) show the evolution of the gapless and gapped edge modes and depicts the way it affects the existence of corner states of the system. Pair of in-gap edge modes (denoted by red lines) indicates the existence of second order topological phase, while chiral edge modes (blue lines) signify the existence of first order topological phase. Density of states are shown in the side panel of each edge state diagram.

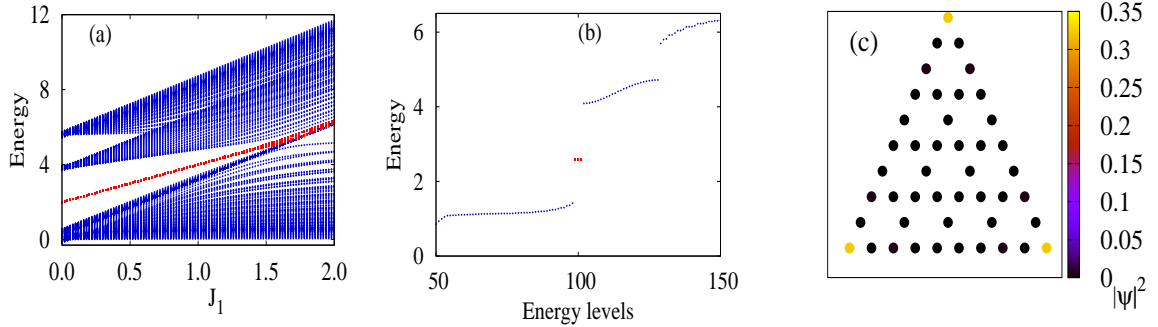


FIG. 5: (color online) (a) Energy spectrum of breathing kagome lattice with varying J_1 for $L = 15$. D_1 , D_2 and J_2 are kept constant at the values of 0.1, 1.5 and 1.0, respectively. Upto $J_1 = 1.6$, zero dimensional corner states exist (denoted by red dots) and beyond this, it decays into the bulk. (b) Energy of the same system is plotted with respect to energy levels for $J_1 = 0.3$. Three red dots at same energy (same value as in the case with zero DMI) show the states at the three corners of the finite triangle. The diagram is truncated for better resolution of the three corner states. (c) Probability distribution of a particular eigenstate corresponding to a corner state energy for $J_1 = 0.2$ and $L = 5$. It shows that the states are indeed localized at the corners and introduction of DM interaction has not changed the distribution considerably.

D_2 , where D_1 is kept fixed at 0.1. To explain the phase diagram, let us fix the value of D_2 at 0.9. Along this line, the system is topologically trivial insulator in first order in the region $0.00 < J_1 \leq 0.41$. Additionally, the system is found to host second order topological phase in the same region since there is a pair of in-gap edge modes in the upper band gap. At $J_1 = 0.42$ lower gap

vanishes. Thereafter, the system hosts a TMI phase with $C_n = (-1, 1, 0)$ up to $J_1 = 0.97$. Thus, the system becomes topologically nontrivial in first order for $0.42 < J_1 \leq 0.97$. But, at the same time, the gapped pair of edge mode in the upper band gap changes its shape in such a manner that the lower edge mode decays into bulk as it is shown in Fig 7. Because of

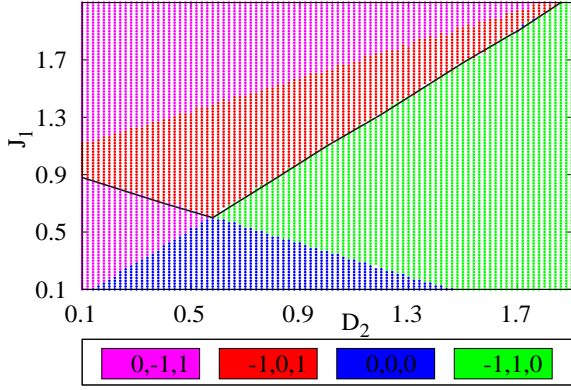


FIG. 6: (color online) Topological phase diagram in $J_1 - D_2$ parameter space with $J_2 = 1.0$ and $D_1 = 0.1$. Four different phases are separated by different colors as shown in the lower panel. In first order, three of them are topologically nontrivial and one is trivial. The solid black line separates topologically nontrivial (lower portion) and trivial (upper portion) phases in second order. Evidently, green and magenta portions beneath the solid black line host both first and second order topological nontrivial phases.

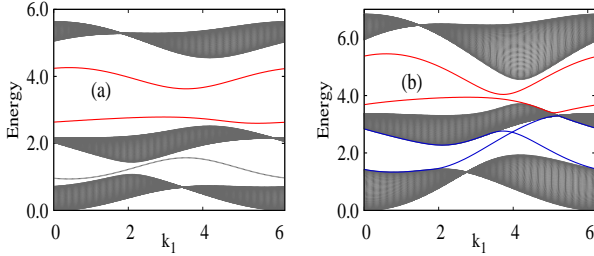


FIG. 7: (color online) Edge state diagram for $D_1 = 0.1$, $D_2 = 0.9$ and (a) $J_1 = 0.3$, (b) $J_1 = 0.7$. Upper band-gap hosts two gapped pair of edge modes (denoted by red lines) in (a), while the lower one decays into the bulk in (b). A chiral edge state appears between the lower band-gap in (b).

this fact, although the value of p_1 for upper band is $1/3$ up to $J_1 = 0.97$, but the corner states are topologically protected up to $J_1 = 0.41$. So, violation of bulk-corner-correspondence rule is noted again in the region $0.42 < J_1 \leq 0.97$. Thus, for $D_1 = 0.1$ and $D_2 = 0.9$, coexistence of both phases remains in the region $0.42 < J_1 \leq 0.97$. For $J_1 > 0.97$, the upper band-gap vanishes and the system undergoes a topological phase transition where it is driven into a phase which is topologically trivial in second order but nontrivial in first order. This TMI phase is characterized by the Chern numbers $(-1, 0, 1)$. With further increase of J_1 , another phase transition is observed at $J_1 = 1.57$. The resulting TMI phase has the Chern number distribution $(0, -1, 1)$.

So, it can be concluded that, although polarization, as a topological invariant, changes its value only when gap closes, its $(d-2)$ dimensional counterpart, the corner states will be found as long as the pair of in-gap edge modes survives distinctly without crossing each

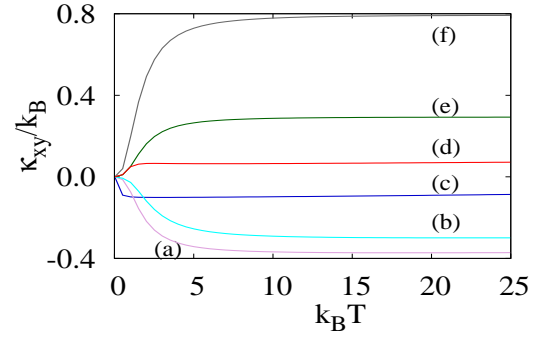


FIG. 8: (color online) Variation of $\kappa_{xy}(T)$ as a function of T for $J_2 = 1.0$ and (a) $J_1 = 1.7$, $D_1 = 0.1$, $D_2 = 1.5$, for $C_n = (-1, 0, 1)$, (b) $J_1 = 2.2$, $D_1 = 0.1$, $D_2 = 1.5$, for $C_n = (0, -1, 1)$, (c) $J_1 = 0.2$, $D_1 = 0.1$, $D_2 = 1.5$, for $C_n = (-1, 1, 0)$, (d) $J_1 = 1.3$, $D_1 = -1.4$, $D_2 = 0.3$, for $C_n = (1, -1, 0)$, (e) $J_1 = 1.3$, $D_1 = 0.0$, $D_2 = -0.2$, for $C_n = (0, 1, -1)$, (f) $J_1 = 1.4$, $D_1 = -0.5$, $D_2 = -0.8$, for $C_n = (1, 0, -1)$.

other or decaying into bulk band in $(d-1)$ dimension. Thus, there is an anomaly in the correspondence between two-dimensional bulk and its zero-dimensional boundary for the SOTMI phase. In addition, this diagram clearly exhibits the occurrence of phase transitions between different topological phases with the variation of parameters, J_1 and D_2 .

V. THERMAL HALL CONDUCTIVITY

The values of thermal Hall conductivity (THC) of the system have been calculated for first order TMI phases. THC is useful to study the occurrence of phase transitions, and, at the same time, these values can be verified experimentally. Resulting diagram is shown in Fig 8. We have included THC values for some extra TMI phases those are not discussed before. Additional TMI phases with different combinations of Chern numbers are obtained by varying all the parameters. The transverse THC can be formulated in terms of Berry curvatures, $\Omega_n(\mathbf{k})$ as⁴⁴,

$$\kappa_{xy}(T) = -\frac{k_B^2 T}{4\pi^2 \hbar} \sum_n \iint_{\text{1BZ}} c(\rho_n(\mathbf{k})) dk_x dk_y \Omega_n(\mathbf{k}). \quad (8)$$

Here the sum runs over all bands, n . k_B is the Boltzmann constant and \hbar is the reduced Planck's constant. $\rho_n(\mathbf{k}) = 1/(e^{E_n(\mathbf{k})/k_B T} - 1)$ is the Bose distribution function with $E_n(\mathbf{k})$ being the energy eigenvalue of the n -th band. $c(x) = (1+x) \ln\left(\frac{1+x}{x}\right)^2 - (\ln x)^2 - 2Li_2(-x)$ where $Li_2(y) = -\int_0^y dz \frac{\ln(1-z)}{z}$. In high temperature limit, THC can be simplified as $\kappa_{xy} = -\frac{k_B}{4\pi^2 \hbar} \sum_n C_n \bar{E}_n$ ²⁹, where the \mathbf{k} -dependent energy is replaced by the average energy of the respective band. By using this equation and the distribution of Chern numbers, one can anticipate the sign of saturated value of κ_{xy} at high temperature. For example,

sign will be positive (negative) if the band with higher energy has lower (higher) value of Chern number considering one of the bands always has $C_n = 0$ in this three-band system. The behavior of THC is reflected in Fig. 8.

VI. SUMMARY AND DISCUSSIONS

We have investigated the properties of FM Heisenberg model with and without DMI on breathing kagome lattice and established the simultaneous appearance of first and second order TMI phases for various values of the exchange and DMI strengths which have been taken of different magnitudes for upward and downward triangles. Topological phase diagram of breathing kagome ferromagnet is richer than that of kagome. Magnon dispersion relations are obtained following LSWT for any value of spin S . While only a single SOTMI phase exists when no DMI is present, either SOTMI or TMI or both of them are present for non-zero DMI strength. In order to characterize the first order conventional TMI phases the Chern numbers of the insulating band as well as chiral edge states in strip geometry are obtained. The existence of different phases with different distribution of Chern numbers and the transition between them are studied. Transverse THC values for various TMI phases are also calculated. While SOTMI phases are characterized by

non-zero values of polarization or in terms of the coordinate of Wannier center, those are additionally verified by the existence of zero-dimensional corner states where the pair of in-gap edge modes are clearly found in one dimension without any crossing. In previous studies on breathing kagome lattice, SOTI phase was found in a fermionic tight binding model¹³. A TI phase was found on another tight binding model in the presence of spin orbit coupling⁴⁵.

Six different TMI phases and one SOTMI phase are found in this system. Since the TMI phase in kagome ferromagnet has been observed before in $\text{Lu}_2\text{V}_2\text{O}_7$ ^{30,31}, these findings can also be verified experimentally in future. No material is available right now whose property can be explained in terms of FM breathing kagome lattice. DMI can be induced via external electric field if it is not present intrinsically²⁹. Topological phases with higher Chern numbers may be obtained by introducing further neighbor interactions. Similarly, it would be more interesting to study the topological behavior of the FM models on three-dimensional pyrochlore lattice by following the same procedure. Violation of bulk-corner-correspondence rule found in some SOTMI phases demands more attention as well. Anomaly in bulk-corner-correspondence rule is reported before in a Hubbard model on kagome lattice, where gapless spin excitations around the corners are found in the presence of electron correlations instead of gapless charge excitations³⁹.

-
- * Electronic address: arghyasil36@gmail.com
 † Electronic address: asimkumar96@yahoo.com
- ¹ Haldane F. D. M., Phys. Rev. Lett. **61**, 2015 (1988).
 - ² Thouless D. J., Kohomoto M., Nightingale P. and den Nijs M., Phys. Rev. Lett. **49**, 405 (1982).
 - ³ Hasan M. Z. and Kane C. L., Rev. Mod. Phys. **82**, 3045 (2010).
 - ⁴ Hatsugai Y., Phys. Rev. Lett. **71**, 3697 (1993).
 - ⁵ Hatsugai Y., Phys. Rev. B **48**, 11851 (1993).
 - ⁶ T. Morimoto, A. Furusaki, Phys. Rev. B **88**, 125129 (2013).
 - ⁷ Benalcazar W. A., Bernevig B. A., and Hughes T. L., Science **357**, 61 (2017).
 - ⁸ Benalcazar W. A., Bernevig B. A., and Hughes T. L., Phys. Rev. B **96**, 245115 (2017).
 - ⁹ Peng Y., Bao Y., and Von Oppen F., Phys. Rev. B **95**, 235143 (2017).
 - ¹⁰ J. Langbehn, Y. Peng, L. Trifunovic, F. von Oppen, and P. W. Brouwer, Phys. Rev. Lett. **119**, 246401 (2017).
 - ¹¹ Song Z., Fang Z., and Fang C., Phys. Rev. Lett. **119**, 246402 (2017).
 - ¹² F. Schindler, A. M. Cook, M. G. Vergniory, Z. Wang, S. S. P. Parkin, B. A. Bernevig, and T. Neupert, Science Advances **4**, 0346 (2018).
 - ¹³ M. Ezawa, Phys. Rev. Lett. **120**, 026801 (2018).
 - ¹⁴ R. Seshadri, A. Dutta, and D. Sen, Phys. Rev. B **100**, 115403 (2019).
 - ¹⁵ M. Geier, L. Trifunovic, M. Hoskam and P. W. Brouwer, Phys. Rev. B **97**, 205135 (2018).
 - ¹⁶ T. Liu, Y. R. Zhang, Q. Ai, Z. Gong, K. Kawabata, M. Ueda and F. Nori, Phys. Rev. Lett. **122**, 076801 (2019).
 - ¹⁷ V. Dwivedi, C. Hickey, T. Eschmann and S. Trebst, Phys. Rev. B **98**, 054432 (2018).
 - ¹⁸ Z. Li, Y. Cao, P. Yan and X. Wang, Npj Comput. Mater. **5**, 107 (2019).
 - ¹⁹ B. Y. Xie, H. F. Wang, H.-X. Wang, X. Y. Zhu, J.-H. Jiang, M. H. Lu, and Y. F. Chen, Phys. Rev. B **98**, 205147 (2018).
 - ²⁰ T. Fukui, Phys. Rev. B **99**, 165129 (2019).
 - ²¹ H. Wakao, T. Yoshida, H. Araki, T. Mizoguchi, and Y. Hatsugai, arXiv:1909.02828
 - ²² H. Araki, T. Mizoguchi and Y. Hatsugai, arXiv:1906.00218.
 - ²³ M. Serra-Garcia, V. Peri, R. Ssstrunk, O. R. Bilal, T. Larsen, L. G. Villanueva, and S. D. Huber, Nature **555**, 342 (2018).
 - ²⁴ S. Imhof, C. Berger, F. Bayer, J. Brehm, L. W. Molenkamp, T. Kiessling, F. Schindler, C. H. Lee, M. Greiter, T. Neupert, and R. Thomale, Nat. Phys. **14**, 925 (2018).
 - ²⁵ L. Zhang, J. Ren, J.S. Wang and B. Li, Phys. Rev. B **87**, 144101 (2013).
 - ²⁶ S. A. Owerre, Phys. Rev. B **95**, 014422 (2017).
 - ²⁷ S. A. Owerre, J. Phys. Commun. **1**, 021002 (2017).
 - ²⁸ R. Seshadri and D. Sen, Phys. Rev. B **97**, 134411 (2018).
 - ²⁹ X. Cao, K. Chen and D. He, J. Phys.: Condens. Matter **27**, 166003 (2015).
 - ³⁰ Y Onose, T Ideue, H Katsura, Y Shiomi, N Nagaosa and Y Tokura, Science, **329**, 297 (2010).
 - ³¹ H Katsura, N Nagaosa and P A Lee, Phys. Rev. Lett.

- 104**, 066403 (2010).
- ³² R. Chisnell, J. S. Helton, D. E. Freedman, D. K. Singh, R. I. Bewley, D. G. Nocera, and Y. S. Lee, *Phys. Rev. Lett.* **115**, 147201 (2015).
- ³³ L. Chen, J. -H. Chung, B. Gao, T. Chen, M. B. Stone, A. I. Kolesnikov, Q. Huang, and P. Dai, *Phys. Rev. X* **8**, 041028 (2018).
- ³⁴ M. Hirschberger, R. Chisnell, Y. S. Lee, and N. P. Ong, *Phys. Rev. Lett.* **115**, 106603 (2015).
- ³⁵ D. G. Joshi, *Phys. Rev. B* **98**, 060405(R) (2018).
- ³⁶ M. Deb and A. K. Ghosh, *J. Phys.: Condens. Matter* **31**, 345601 (2019).
- ³⁷ H. Xue, Y. Yang, F. Gao, Y. Chong and B. Zhang, *Nature Materials* **18**, 108 (2019).
- ³⁸ X. Chen, W. M. Deng, F.L. Shi, F. L. Zhao, M. Chen, and J. W. Dong, *Phys. Rev. Lett.* **122**, 233902 (2019).
- ³⁹ K. Kudo, T. Yoshida and Y. Hatsugai, *Phys. Rev. Lett.* **123**, 196402 (2019).
- ⁴⁰ M. Ezawa, *Phys. Rev. B* **98**, 201402(R) (2018).
- ⁴¹ C. W. Peterson, W. A. Benalcazar, T. L. Hughes and Bahl, *Nature* **555**, 346350 (2018).
- ⁴² A. El Hassan, F. K. Kunst, A. Moritz, G. Andler, E. J. Bergholtz, and M. Bourennane, *Nature photonics* **13**, 697 (2019).
- ⁴³ T. Fukui, Y. Hatsugai and H. Suzuki, *J. Phys. Soc. Jpn.* **74**, 1674 (2005).
- ⁴⁴ R. Matsumoto and S. Murakami, *Phys. Rev. Lett.* **106**, 197202 (2011).
- ⁴⁵ A. Bolens and N. Nagaosa, *Phys. Rev. B* **99**, 165141 (2019).